Defects and Nanocrystals Generated by Si Implantation into a-SiO_2

C. J. Nicklaw, M. P. Pagey, S. T. Pantelides, D. M. Fleetwood, R. D. Schrimpf, K. F. Galloway, J. E. Wittig, B. M. Howard, E. Taw, W. H. McNeil, and J. F. Conley, Jr.

***Abstract*—Electrical charge-trapping characteristics have been studied in thermal oxides that were implanted with Si, experimentally using electron spin resonance (ESR), capacitance versus voltage (CV) measurements, transmission electron microscopy (TEM), atomic force microscopy (AFM), and theoretically with Density Functional Theory (DFT) using plane waves. Our study examines possible defect structures associated with excess Si in thermal oxides.**

I. Introduction

SILICON dioxide (SiO_2) has useful optical and electrical properties enabling many diverse scientific and technological applications from optical wave-guides to semiconductor devices. The use of SiO_2 as isolation layer for device manufacturing and as the buried isolation layer for silicon-on-insulator (SOI) technology has led to the need to understand defects and their precursors [1], [2] and their relationship to processing [3]. Buried SiO_2 layers formed by oxygen ion implantation have been examined structurally [4], [5], by varying process conditions [6], resulting in novel manufacturing techniques [2]. The micro-characterization of the defect structure of SiO_2 is essential as many advanced technological applications operate in harsh external environments. Knowledge of the microscopic defect structure influencing the optical and electronic properties of SiO_2 allows optimization of the manufacturing, design and operation of the applications. In addition, investigation of the defect structure of amorphous SiO_2 and the effect of manufacturing processes on these properties provides insight into the fundamental interactions between electrons and holes in wide band gap materials. In an attempt to better understand the charge characteristics of oxygen deficient centers and excess Si within an a-SiO_2 matrix we implanted Si into thermally grown oxide. Experimental work is examined physically (ESR, TEM, AFM) and electrically (CV). Theoretical analysis has been presented to explain the atomic structure of the defects created by excess Si.

Manuscript received July 25, 2000.

C. J. Nicklaw, M. P. Pagey, S. T. Pantelides, D. M. Fleetwood, R. D. Schrimpf, K. F. Galloway, and J. E. Wittig are with Vanderbilt University, Nashville, TN 37235 USA (e-mail: chris@drcsdca.com).

B. M. Howard, E. Taw, and W. H. McNeil are with Dynamics Research Corporation, San Diego, CA 92106 USA.

J. F. Conley, Jr. was with the Dynamics Research Corporation, San Diego, CA 92106 USA. He is now with the NASA Jet Propulsion Laboratory, Pasadena, CA 91109 USA.

Publisher Item Identifier S 0018-9499(00)11257-2.

II. Experimental Details

A. Oxide Samples

The 5500 Å thick oxides used in this study were grown in steam at 950°C on 15–25 ohm-cm boron doped $\langle 100 \rangle$ silicon wafer substrates. The oxides were then implanted with $1 \times 10^{16}/\text{cm}^2$, $5 \times 10^{16}/\text{cm}^2$, $1 \times 10^{17}/\text{cm}^2$, and $5 \times 10^{17}/\text{cm}^2$ Si^+ at 180 keV and then subsequently annealed for 60 min in N_2 at either 900°C or 1000°C. An average Si^+-peak depth of 2700 Å in the oxide with a straggle of ~800 Å was calculated by SRIM [7] software for these implants. The implants were performed at the IC Implant Center, Sunnyvale, CA. The average beam current during the implantation was 11.9 mA and the wafers were placed on a chuck that was actively cooled with 10°C water. The estimated average temperature of the wafers during the implant was 100–130°C. A set of oxide samples was neither implanted nor annealed and served as the control set.

B. Physical Characterization

ESR measurements were performed at room temperature on a state of the art Bruker Instruments ESP300E x-band spectrometer. Estimates of spin density and g-value were made by comparison with a calibrated "weak-pitch" spin standard. Absolute accuracy of spin densities is estimated to be better than a factor of two; relative accuracy is estimated to be approximately 10%. TEM was performed on a Philips system while AFM was accomplished on a Digital Instruments, Dimension™ 3100AFM in TappingMode™/Phase.

C. Electrical Characterization

The electrical behavior of defects in the oxides was characterized by observing the trapping of electrons and holes in the oxide. Electron-hole pairs were generated in the oxide through exposure to ultraviolet light (10.2 eV photons from a deuterium source in vacuum, VUV). The VUV exposure is expected to generate electron-hole pairs only in a ~100 Å surface layer of the oxide. In order to isolate the effect of electron trapping, a negative corona bias was applied to the top of the oxide. Under the applied negative corona bias, the photo-generated electrons drift away from the surface of the oxide and interact with defects throughout the bulk of the oxide while the holes are promptly swept out of the oxide by recombination with electrons at the surface of the oxide. This recombination results in a change in the corona bias which can be used to estimate the total number of electron-hole pairs generated in the oxide. This set of experiments will be referred to as "electron-trapping phase" in the rest

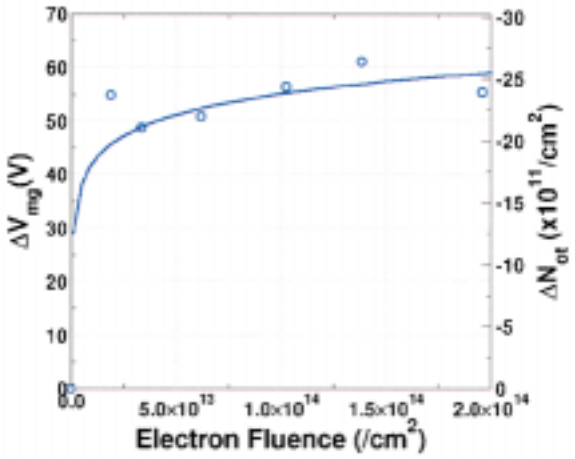

Fig. 1. The change in V_{mg} as a function of electron fluence during the first electron trapping phase of the carrier trapping experiments on a sample implanted with $5 \times 10^{17}/\text{cm}^2$ Si^+ and annealed at 1000°C. This figure shows the saturation of available electron traps as early as a fluence of $\sim 2 \times 10^{13}\text{C/cm}^2$.

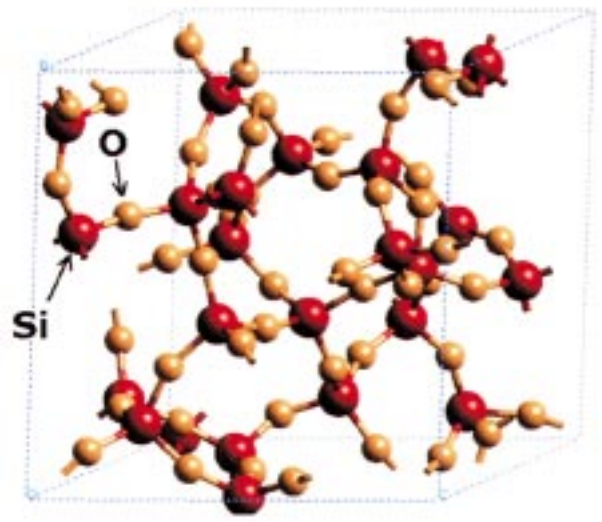

Fig. 2. Base structure used for simulation. This structure represents an amorphous SiO_2 cell.

of the text. Similarly, experiments were performed with a positive corona bias in order to observe the effect of hole-trapping in the oxide (hole-trapping phase). The effective density of trapped charge in the oxide was calculated from the shift in midgap voltage (V_{mg}) extracted from high-frequency (1 MHz) CV characteristics of the samples using a HP 4284A CV meter and a mercury probe. The accuracy of these measurements is expected to be approximately 15%.

Each set of oxides was first subjected to the electron-trapping phase to an electron fluence of approximately $2 \times 10^{14}/\text{cm}^2$ measured by monitoring the decay in the corona bias. The CV characteristics of the oxides were measured periodically during this phase. The CV curves stopped changing appreciably at this maximum fluence, indicating that almost all the available traps were filled at the end of this trapping phase (Fig. 1). This was followed by a hole-trapping phase to the same fluence and, finally, another identical electron-trapping phase.

III. Computational Details

The study of defects produced by Si^+ implantation into amorphous SiO_2 is addressed by *ab initio* calculations using DFT [8]. Unlike conventional quantum theory, where the system's ground state energy is calculated as a function of many electron wave functions, DFT calculates the system energy as a function of the electron density. The significance of this ground state energy calculation is that nearly all physical properties of a system can be related to its total energy and systems can be compared through the difference between their total energies. The use of electron density to describe the system's properties in DFT allows one to separate the Schröinger equation for a many-electron system with interacting electrons into a set of independent one-electron Schrödinger equations. The details of the DFT-based approach can be found in the Appendix.

The geometry of the system is selected such that both long and short range environments of the defects introduced can be taken into account with the same level of accuracy. The computational advantage in this approach is that the use of periodic boundary conditions allows the electron wavefunctions to be expanded in terms of plane waves.

Our theoretical work was done using a base amorphous SiO_2 (a-SiO_2) structure shown in Fig. 2. This structure, S_0, a base 72 atom unit cell, with a volume of 1122.79 Å^3 and a density of 2.13 g/cm^3, was confirmed to be a valid representation of the a-SiO_2 molecular structure by comparing it with the results reported by M. Boero *et al.* [9]. The theoretical bandgap was calculated for S_0 and used as the baseline to compare the generated defect structures' energy state. Four variations based on S_0 were generated in an attempt to examine possible defects in Si implanted a-SiO_2. No attempt was made in this work to model the implantation process. The structures generated were:

- $\mathbf{S_1}$: S_0 with an oxygen vacancy and an excess Si atom in the unit cell,
- $\mathbf{S_2}$: S_0 with an oxygen vacancy, an excess Si atom near the vacancy, and an oxygen atom at a distance of approximately 3 Å from the vacancy,
- $\mathbf{S_3}$: S_0, an oxygen vacancy with an excess Si atom near the vacancy, and an oxygen atom at a distance of approximately 2 Å from the vacancy, and
- $\mathbf{S_4}$: S_0 with an excess Si atom placed within the cell.

These four starting structures were chosen as possible conditions that could exist in a-SiO_2 after Si^+ implantation. The structure S_1 represents an implanted Si atom interacting with an oxygen vacancy which is known to be present in as-grown as well as implanted thermal oxides [10]. Structures S_2 and S_3 represent results of collisions between implanted Si and oxygen in a-SiO_2 during the implantation. Finally, structure S_4 represents an implanted Si atom coming to rest or diffusing into a region with no pre-existing defects. The bandgap of the base S_0 structure was calculated to be 5.74 eV. This is smaller than the experimental value of a-SiO_2 of ~8.9 eV. The difference of 3.14 eV can be attributed to the approximations involved in using the DFT approach. Using this theoretically calculated bandgap value means our calculated defect energy states are accurate within this framework but provide only a relative

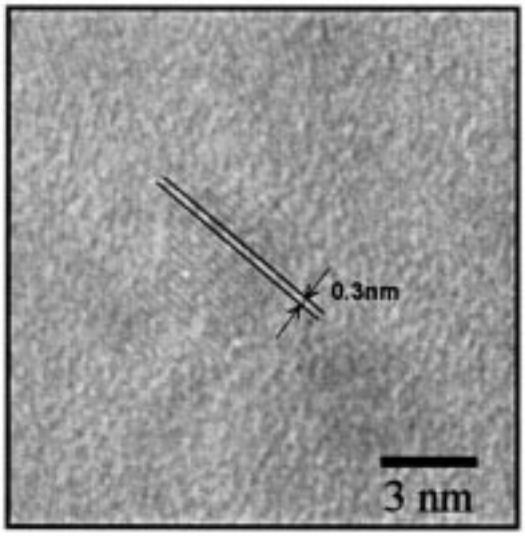

Fig. 3. TEM photomicrograph of a SiO_2 sample implanted with $5\times10^{17}/cm^2$ Si^+ and annealed at 1000° showing Si nanocrystal formation.

picture of the positions of their energy states within as-processed a-SiO_2. Once the theoretical bandgap was established for possible defect structures, ground state energy, $E(N)$, and energy in the first excited state, $E(N+1)$, were calculated.

IV. Results and Discussion

A. Physical Analysis

Physical analysis of silicon implanted a-SiO_2 was done after annealing at 900 and 1000°C and compared to the as-grown control oxide. The above anneal temperatures and implant parameters were chosen for comparison with published work on photoluminescence of Si-nanocrystals grown by Si^+ implantation into a-SiO_2. SiO_x nodules were seen at all doses ($1\times10^{16}/cm^2$, $5\times10^{16}/cm^2$, $1\times10^{17}/cm^2$, and $5\times10^{17}/cm^2$) after the anneals at 900 and 1000°C. Fig. 3 shows a TEM analysis of the Si-nanocrystals within a SiO_x matrix after a $5\times10^{17}/cm^2$ implant and 1000°C anneal. Similar results are also reported in [4], [11].

AFM analysis of the excess Si structures also showed SiO_x nodule growth at all doses (Fig. 4). After $5\times10^{17}/cm^2$ implant and 1000°C anneal the AFM was able to delineate grain boundaries and difference in material. This helps confirm current research pointing to Si-nanocrystal formation at 1000°C [4], [11]. The series of AFM phase images shown in Fig. 4 show that SiO_x nodule size increases with Si^+ dose and annealing temperature. This evidence, as well as an increase in SiO_x size with annealing time, agrees with work done in [12].

In our ESR analysis, we build upon the previous work relating various paramagnetic defects created by VUV, ^{60}Co, or X-ray irradiation [2], [3], [5], [6], [10]. The defects seen in the Si^+ implanted and annealed thermal oxides are the classic E'_γ, amorphous Si D-centers ($Si_3 \equiv Si^{\uparrow}$), and P_b-centers at the Si–SiO_2 interfaces [2], [3], [5], [6], [10], [13], [14]. In Fig. 5, we grouped our ESR spectra for the control and implanted samples ($1\times10^{16}/cm^2$ dose, 900°C anneal) before and after the electron trapping phase described in Section II-C. The value of

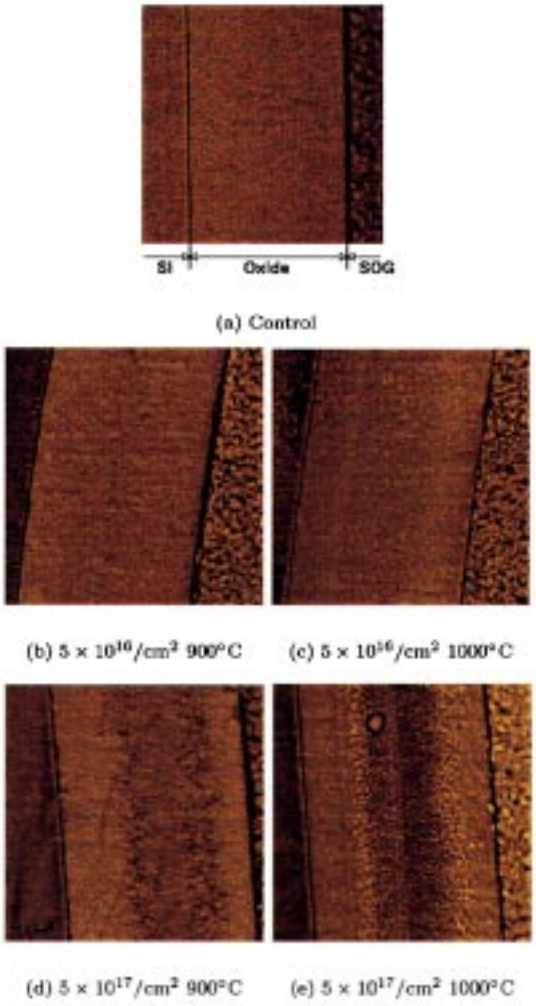

Fig. 4. A series of AFM phase images showing increased SiO_x nodule formation with implant dose and anneal temperature. A spin-on glass (SOG) layer was used on top of the oxides as part of the sample preparation for AFM measurements.

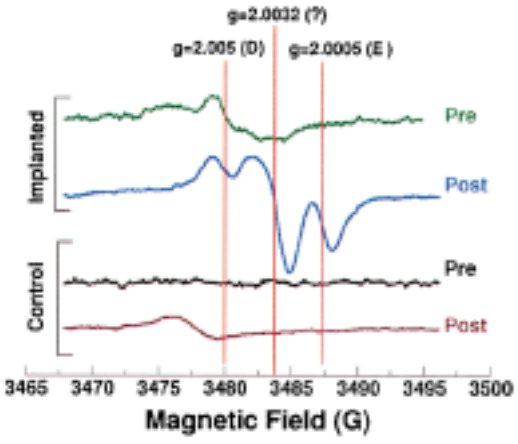

Fig. 5. ESR traces with three g-values mapped to corresponding defects in the implanted ($1\times10^{16}/cm^2$ and annealed at 900°C) and control samples after electron trapping.

ESR is seen in the traces for the implanted samples. In particular, as seen in Fig. 5, three g-values stand out—at $g=2.0005$ the classic E'_γ signal, $g=2.005$ associated with D-centers,

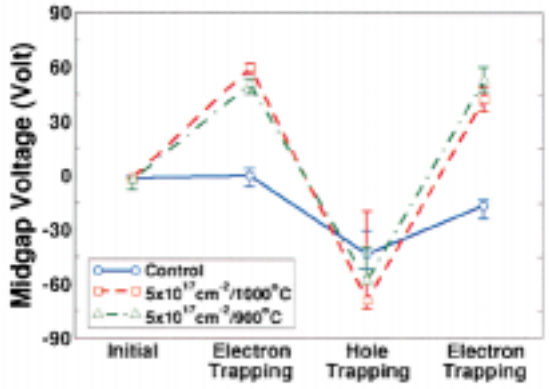

Fig. 6. The density of trapped charge in the oxide during carrier trapping experiments. The figure shows the trapped charge density at the end of each phase of the experiment.

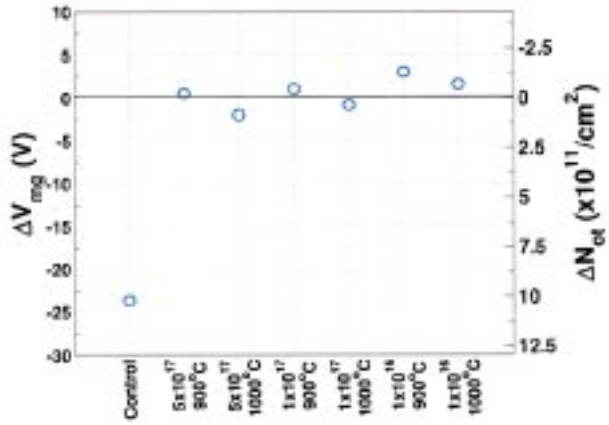

Fig. 7. The shift in midgap voltage in the implanted samples after VUV-exposure for 30 min. without any bias.

and finally one at $g = 2.0032$. This last g-value has been associated with various defects in Si-rich oxides [10], [13], [14]. Defect structures for this center have recently been proposed by Bratus *et al.* [14] and Karna *et al.* [13] such as $OSi_2 \equiv Si^{\uparrow}$ and $O_2Si \equiv Si^{\uparrow}$. The occurrence of Si dangling bond defects in non-stoichiometric regions has been shown in our theoretical work as well as others [13]. These defects are possibly the precursors to silicon nanocrystals in an a-SiO_2 matrix.

B. Electrical Characterization

The variation in the midgap voltage of the control samples during the carrier trapping experiments described in Section II-C is compared with those of the implanted samples in Fig. 6. The results for samples implanted with $5 \times 10^{17}/\text{cm}^2$ dose of Si^+ and anneal at 900°C and 1000°C are shown in this figure. The data points indicate the midgap voltage at the end of each carrier-trapping phase.

As seen from the V_{mg} values at the end of the first electron-trapping phase, the implanted oxides show significantly more electron trapping (increase in V_{mg}) as compared to the control samples, which show negligible shift in V_{mg} during this phase. This confirms that the silicon implant results in generation of electron traps in the oxide which are not present in the control samples. The value of V_{mg} at the end of the hole-trapping phase indicates that these electron traps can be neutralized (through compensation or annihilation) by hole trapping in the oxide [1]. Furthermore, a net negative value of V_{mg} after this phase implies the presence of trapped holes in the oxide. The values of V_{mg} after the hole-trapping phase are almost identical in the implanted and control devices. This indicates that the Si^+ implantation does not result in a significant change in the density of hole traps in these oxides. Finally, the second electron trapping phase brings the V_{mg} very close to its value after the first electron trapping phase, indicating that most of the electron and hole traps present in the implanted oxides as well as the control oxides are reversible.

The average density of interface traps was also extracted from the CV characteristics during these experiments. No significant change in the interface trap density was observed during any of the carrier trapping phases in any of the oxides.

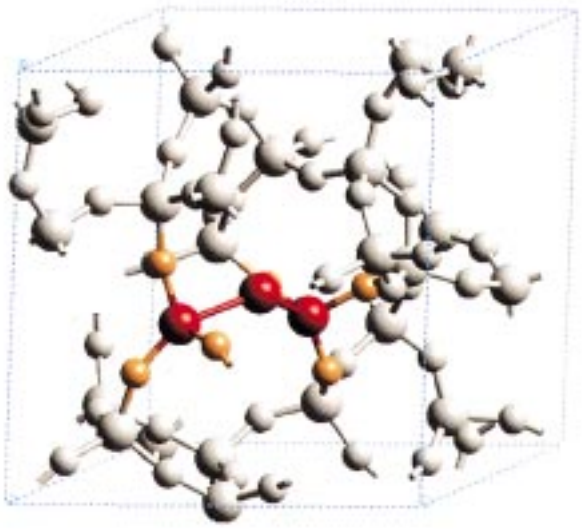

Fig. 8. Ground state structure obtained from the S_1 cell, the $\equiv$ Si $-$ Si $-$ Si $\equiv$ defect.

In order to observe the behavior of the samples when both electrons and holes are available for trapping, we subjected the samples to VUV exposure without any corona bias. The change in V_{mg} at the end of the VUV exposure is shown in Fig. 7. As seen from this figure, the control samples accumulate a significant amount of positive charge during this experiment. However, the presence of both electron and hole traps in the implanted oxides results in almost no net change in V_{mg} in these samples.

C. Theoretical Analysis

When structure, S_1, was allowed to relax to ground state, $E(N)$, the resulting defect structure is a doubly coordinated Si atom, $\equiv$ Si $-$ Si $-$ Si $\equiv$ (also known as a double oxygen vacancy) as depicted in Fig. 8. From this structure the first excited state energy, $E(N+1)$, was calculated.

The next series of defects we considered were oxygen atom displacements near (<2 Å) and far (>3 Å) from their base

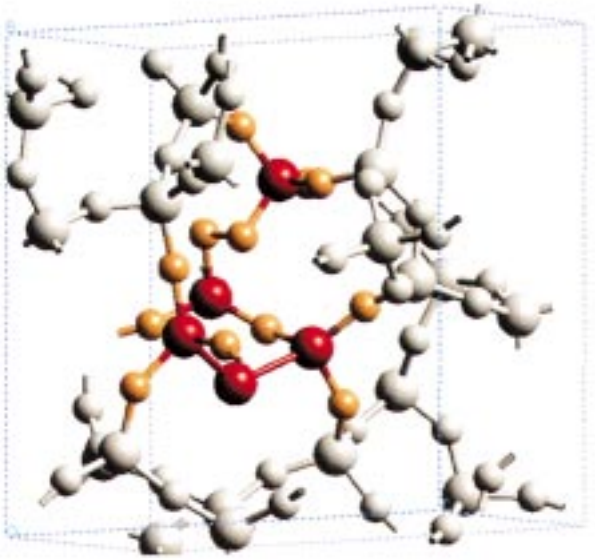

Fig. 9. Ground state structure obtained from the S_2 cell, the double defect structure $\equiv$ Si $-$ O $-$ O $-$ Si $\equiv$ and $\equiv$ Si $-$ Si $-$ Si $\equiv$.

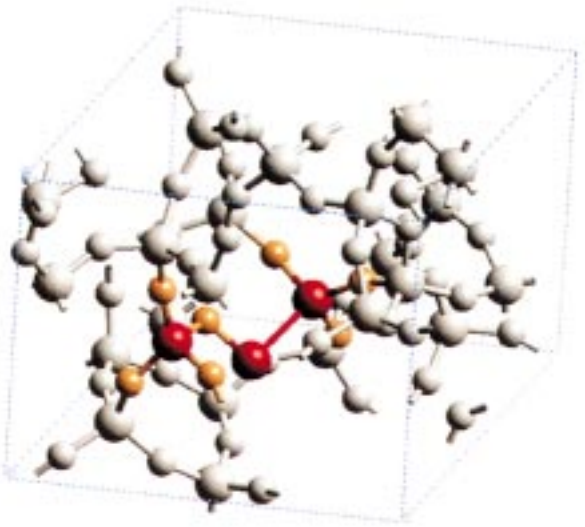

Fig. 10. Ground state structure obtained from the S_3 cell, the $\equiv$ Si $-$ O $-$ Si $-$ Si $\equiv$ defect.

a-SiO_2 position. Such displacement is expected in implanted samples as a result of kinetic energy transfer from the implanted Si atoms. An oxygen atom was displaced (far for S_2 and near for S_3) and a Si atom added to the base a-SiO_2 structure. These structures were allowed to relax to their respective ground states, $E(N)$. The resulting configurations is a double defect (far) a $\equiv$ Si $-$ O $-$ O $-$ Si $\equiv$ and a $\equiv$ Si $-$ Si $-$ Si $\equiv$ (starting from S_2) and a defect structure of $\equiv$ Si $-$ O $-$ Si $-$ Si $\equiv$ (starting from S_3) as shown in Figs. 9 and 10. These defect structures were excited to $E(N+1)$ and the state calculated for each defect. Another situation that could arise is silicon diffusing into a-SiO_2 with no defects. When condition S_4 was allowed to relax to ground state it produced the defect $OSi_2 \equiv$ Si, a Y-center [13]. The results are shown in Fig. 11. $E(N+1)$ was also calculated for this structure.

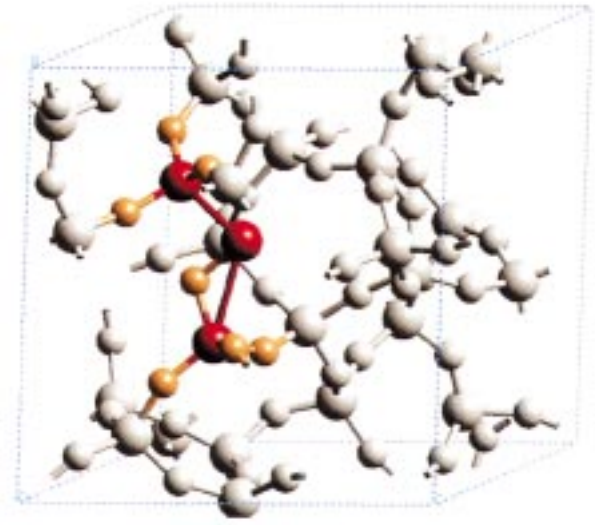

Fig. 11. Ground state structure obtained from the S_4 cell, the $OSi_2 \equiv$ Si defect.

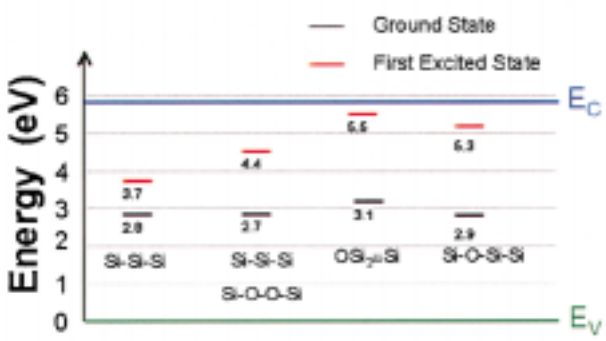

Fig. 12. The calculated energy states of the various defects in the theoretical SiO_2 bandgap.

Examining the results shown in Fig. 12 that the doubly coordinated Si atom is the most stable defect in its excited state. This defect is also referred to as the double oxygen vacancy. The double defect structure $\equiv$ Si$-$O$-$O$-$Si $\equiv$ and $\equiv$ Si$-$Si$-$Si $\equiv$ is probably produced by an Si atom colliding with an oxygen and kinetically displacing it to a distance more than 3 Å. This conclusion is supported by the ground state energy of this structure being 7 eV higher than the ground states of S_3 and S_4. The 7 eV difference is an energy barrier that must be overcome if Si was to replace an oxygen atom by any other means besides kinetic energy transfer. This possible defect structure like the doubly coordinated Si atom ($\equiv$ Si $-$ Si $-$ Si $\equiv$) is very reactive having an excited state well within the calculated bandgap.

The other defect structures, $OSi_2 \equiv$ Si and $\equiv$ Si $-$ O $-$ Si $-$ Si $\equiv$, have ground states within the bandgap, but their respective excited states $E(N+1)$ are very close the conduction band edge $\sim$0.50 eV making $OSi_2 \equiv$ Si and $\equiv$ Si $-$ O $-$ Si $-$ Si $\equiv$ shallow states.

V. Conclusion

Physical analysis by TEM and AFM show that samples implanted with excess Si at doses between

$1 \times 10^{16}/\text{cm}^2$–$5 \times 10^{17}/\text{cm}^2$ and then annealed at 900°C or 1000°C show SiO_x nodule growth. Si nanocrystals were observed in the sample implanted with Si dose of $5 \times 10^{17}/\text{cm}^2$ and annealed at 1000°C (Fig. 3). This supports previously published work [4], [11], [15]–[22] on the dependence of the density of Si nanocrystals and their precursor SiO_x nodules on the implantation dose, anneal temperature, and anneal time. SiO_x nodules increase in size and eventually go to nanocrystal Si as the implant dose increases and/or annealing temperature and/or annealing time increases. This is an artifact of the excess Si in an a-SiO_2 matrix. Theoretical work presented here examines four possible defect structures that could exist within a Si-rich amorphous SiO_2 matrix. The excess Si creates defects that can capture electrons. These results are supported by charge trapping experiments showing the ability of the modified material to capture electrons without any increase in the hole trap density. The structural defects introduced by Si^+ implant have ground and excited energy states that lie within the energy gap of amorphous SiO_2 . Theoretically we show the formation of $\equiv \text{Si} - \text{O} - \text{Si} - \text{Si} \equiv$, $\equiv \text{Si} - \text{Si} - \text{Si} \equiv$, a dual defect complex, the $\equiv \text{Si} - \text{O} - \text{O} - \text{Si} \equiv$ with $\equiv \text{Si} - \text{Si} - \text{Si} \equiv$ and the $\text{OSi}_2 \equiv \text{Si}$, Y-center [13]. These defect structures all have ground and excited states within the bandgap of a-SiO_2. These defects are some of the possible candidates for the charge compensation seen in Fig. 7.

APPENDIX

The total energy of a system of interacting ions (nuclei of atoms in the system) and electrons is written as:

$$E_{\text{Total}} = E_{\text{ion-ion}} + E_{\text{e-ion}} + E_{\text{e-e}} \tag{1}$$

where

- $E_{\text{ion-ion}}$ represents the interaction energy of the ions with other ions,
- $E_{\text{e-ion}}$ represents the potential energy of interaction between electrons and ions and
- $E_{\text{e-e}}$ represents the kinetic energy of electrons and the potential energy of their interactions with each other.

The first term, $E_{\text{ion-ion}}$ is given by:

$$E_{\text{ion-ion}} = \sum_{A=1}^{M} \sum_{B>A}^{M} \frac{Z_A Z_B}{r_{AB}} \tag{2}$$

where

- $r_{AB} = |\vec{r}_A - \vec{r}_B|$ is the distance between two ions A and B located at $\vec{r}_A$ and $\vec{r}_B$ respectively,
- Z_A and Z_B are the atomic masses of the two ions, and
- M is the total number of ions in the system.

The second term, $E_{\text{e-ion}}$, is given by:

$$E_{\text{e-ion}} = \int_V d^3 r V_{\text{ion}}(\vec{r}) \rho(\vec{r}) \tag{3}$$

where

- $\rho(\vec{r})$ is the electron density,
- V is the volume of the system, and
- $V_{\text{ion}}(\vec{r})$ is the electrostatic potential due to the ions as given by:

$$V_{\text{ion}}(\vec{r}) = -Ze^2 \sum_i \frac{1}{|\vec{r} - \vec{r}_i|} \tag{4}$$

where, $\vec{r}$ is the position of the electron and $\vec{r}_i$'s are the positions of the ions.

The final term, $E_{\text{e-e}}$, in (1) describes the kinetic energy of the electrons and the potential energy of their interactions with each other. Kohn and Sham showed that it is possible to map the many-body problem of an interacting electron gas in the presence of an external potential to an exactly equivalent set of self-consistent single electron equations. In their work, the external potential is like that produced by an arrangement of ion cores. The energy term $E_{\text{e-e}}$ is written in terms of a set of single-particle electron states, Ψ_i, as:

$$E_{\text{e-e}} = 2 \sum_i \int_V d^3 r f_i \Psi_i^*(\vec{r}) \left[-\tfrac{1}{2} \nabla^2 \right] \Psi_i(\vec{r}) + \frac{1}{2} \int_V d^3 r \left\{ \int_V d^3 r' \frac{\rho(\vec{r}) \rho(\vec{r}')}{|\vec{r} - \vec{r}'|} + E_{\text{xc}}[\rho(\vec{r})] \right\} \tag{5}$$

and the electron density, $\rho(\vec{r})$, is given by:

$$\rho(\vec{r}) = 2 \sum_i f_i |\Psi_i(\vec{r})|^2 \tag{6}$$

where f_i is the probability of electron orbital occupation ($0 \leq f_i \leq 1$).

The first term in (5) gives the kinetic energy of a noninteracting electron gas, the second term is the electrostatic potential energy and E_{xc} the exchange-correlation energy.

The many-body wave function has to be antisymmetric under the exchange of any two electrons because they are fermions. This results in a spatial separation for electrons of identical spin which reduces the Coulomb energy of the system. Spatially separating electrons with opposite spin reduces the Coulomb energy at the cost of increasing the kinetic energy, an effect known as correlation. These effects make up the exchange-correlation energy, E_{xc}, which is explicitly included in the total energy expression because electrons are treated as independent particles. The exchange-correlation energy is given by:

$$E_{\text{xc}}[\rho(\vec{r})] = \int_V d^3 r \epsilon_{\text{xc}}[\rho(\vec{r})] \rho(\vec{r}) \tag{7}$$

where $\epsilon_{\text{xc}}[\rho(\vec{r})]$ is the exchange-correlation energy per particle for a homogeneous electron gas of density ρ.

The energy of a system of electrons in an external field produced by a collection of nuclei is given by minimizing the energy function in (1). This is equivalent to solving a set of Kohn–Sham equations comprising a one-particle Schrödinger equation together with a so-called self-consistency condition. The Schrödinger equation links the potential to the electron density:

$$\left[-\tfrac{1}{2} \nabla^2 + V_{\text{ion}}(\vec{r}) + V_H(\vec{r}) + V_{\text{xc}}(\vec{r}) \right] \Psi_i(\vec{r}) = \epsilon_i \Psi_i(\vec{r}). \tag{8}$$

The term $V_H(\vec{r})$ is the electrostatic (Hartree) potential generated by the charge distribution following the wave functions. This potential is given by:

$$V_H(\vec{r}) = \int d^3r' \frac{\rho(\vec{r})}{|\vec{r} - \vec{r}'|} \tag{9}$$

and, $V_{\rm xc}$ is the exchange-correlation potential given by:

$$V_{\rm xc}[\rho(\vec{r})] = \frac{\partial}{\partial \rho(\vec{r})} E_{\rm xc}[\rho(\vec{r})]. \tag{10}$$

When the Kohn–Sham equations are solved self-consistently, such that the occupied states generate the same electron density used to construct the potential, then the ground state density and energy have been found. The total energy is then given by:

$$E_{\rm Total} = 2\sum_i^M f_i \epsilon_i - \frac{1}{2}\int_V d^3r \int_V d^3r' \frac{\rho(\vec{r})\rho(\vec{r}')}{|\vec{r} - \vec{r}'|} - \int_V d^3r V_{\rm xc}(\vec{r})\rho(\vec{r}) + E_{\rm xc} + E_{\rm ion\text{-}ion} \tag{11}$$

ACKNOWLEDGMENT

The authors wish to thank J. Howard and J. Johann for their support and Dr. A. Maiti of Molecular Simulations Inc. for his assistance and the reviewers for their helpful comments.

REFERENCES

[1] J. F. Conley Jr., P. M. Lenahan, and P. Roitman, "Evidence for a deep electron trap and charge compensation in SIMOX oxides," *IEEE Trans. Nucl. Sci.*, vol. 39, pp. 2114–2120, Dec. 1992.

[2] S. T. Liu, L. P. Allen, M. J. Anc, W. C. Jenkins, H. L. Hughes, M. E. Twigg, and R. K. Lawrence, "Reduction of radiation induced back channel threshold voltage shifts in partially depleted SIMOX CMOS devices by using ADVANTOX™ substrates," *IEEE Trans. Nucl. Sci.*, vol. 44, pp. 2101–2105, Dec. 1997.

[3] P. M. Lenahan and J. F. Conley, "A comprehensive physically based predictive model for radiation damage in MOS system," *IEEE Trans. Nucl. Sci.*, vol. 45, pp. 2413–2423, Dec. 1998.

[4] V. V. Afanas'ev, A. Stesmans, A. G. Revesz, and H. L. Hughes, "Structural inhomogeneity and silicon enrichment of buried SiO_2 layers formed by oxygen ion implantation in silicon," *J. Appl. Phys.*, vol. 82, no. 5, pp. 2184–2199, Sept. 1, 1997.

[5] R. K. Lawrence, B. J. Mrstik, H. L. Hughes, and P. J. McMarr, "Radiation induced charge in SIMOX buried oxides: lack of thickness dependence at low applied fields," *IEEE Trans. Nucl. Sci.*, vol. 44, pp. 2095–2100, Dec. 1997.

[6] B. J. Mrstik, P. J. McMarr, R. K. Lawrence, and H. L. Hughes, "A study of the radiation sensitivity of noncrystalline SiO_2 films using spectroscopic ellipsometry," *IEEE Trans. Nucl. Sci.*, vol. 45, pp. 2450–2457, Dec. 1998.

[7] J. F. Ziegler, J. P. Biersack, and U. Littmark, *The Stopping and Range of Ions in Solids*, New York: Pergamon, 1985.

[8] R. G. Parr and W. Yang, *Density Functional Theory of Atoms and Molecules*. Oxford: Oxford University Press, 1989.

[9] M. Boero, A. Pasquarello, J. Sarnthein, and R. Car, "Structure and hyperfine parameters of E_1' centers in α-quartz and in vitreous SiO_2," *Phys. Rev. Lett.*, vol. 78, no. 5, pp. 887–890, Feb. 3, 1997.

[10] W. L. Warren, M. R. Shaneyfelt, J. R. Schwank, D. M. Fleetwood, P. S. Winokur, R. A. B. Devine, W. P. Maszara, and J. B. McKitterrick, "Paramagnetic defect centers in BESOI and SIMOX buried oxides," *IEEE Trans. Electron Dev.*, vol. 40, pp. 1755–1764, Dec. 1993.

[11] F. Iacona, G. Franzo, and C. Spinella, "Correlation between luminescence and structural properties of Si nanocrystals," *J. Appl. Phys.*, vol. 87, no. 3, pp. 1295–1303, Feb. 1, 2000.

[12] T. Shimizu-Iwayama, Y. Terao, A. Kamiya, M. Takeda, S. Nakao, and S. Saitoh, "Correlation of microstructure and photoluminescence for nanometer-sized Si crystals formed in an amorphous SiO_2 matrix by ion implantation," *Nano-Structured Materials*, vol. 5, no. 3, pp. 307–318, Mar.–Apr. 1995.

[13] S. Karna, H. Kurtz, W. Shedd, R. Pugh, and B. Singaraju, "New fundamental defects in a-SiO_2," *IEEE Trans. Nucl. Sci.*, vol. 46, pp. 1544–1552, Dec. 1999.

[14] V. Y. Bratus, M. Y. Valakh, I. P. Vorona, T. T. Petrenko, V. A. Yukhimchuk, P. L. F. Hemment, and T. Komoda, "Photoluminescence and paramagnetic defects in silicon-implanted silicon dioxide layers," *J. Luminescence*, vol. 80, pp. 269–273, 1999.

[15] V. V. Afanas'ev and A. Stesmans, "Photoionization of silicon particles in SiO_2," *Phys. Rev. B*, vol. 59, no. 3, pp. 2025–2034, Jan. 15, 1999.

[16] D. Zhang, R. M. Kolbas, P. D. Milewski, D. J. Lichtenwalner, A. I. Kingon, and J. M. Zavada, "Light emission from thermally oxidized silicon nanoparticles," *Appl. Phys. Lett.*, vol. 65, no. 21, pp. 2684–2686, Nov. 1994.

[17] P. D. Milewski, D. J. Lichtenwalner, P. Mehta, A. I. Kingon, D. Zhang, and R. M. Kolbas, "Light-emission from crystalline silicon and amorphous-silicon oxide (SIOX) nanoparticles," *J. Electron. Materials*, vol. 23, no. 1, pp. 57–62, Jan. 1994.

[18] S. Tong, X. N. Liu, and X. M. Bao, "Study of photoluminescence in nanocrystalline silicon/amorphous silicon multilayers," *Appl. Phys. Lett.*, vol. 66, no. 4, pp. 469–471, Jan. 1995.

[19] A. G. Nassiopoulos, S. Grigoropoulos, E. Gogolides, and D. Papadimitriou, "Visible luminescence from one- and two-dimensional silicon structures produced by conventional lithographic and reactive ion etching techniques," *Appl. Phys. Lett.*, vol. 66, no. 9, pp. 1114–1116, Feb. 1995.

[20] T. Shimizu-Iwayama, K. Fujita, S. Nakao, K. Saitoh, T. Fujita, and N. Itoh, "Visible photoluminescence in Si^+-implanted thermal oxide films on crystalline Si," *Appl. Phys. Lett.*, vol. 65, no. 14, pp. 1814–1816, Oct. 1994.

[21] P. Mutti, G. Ghisloti, S. Bertoni, L. Bonoldi, G. F. Cerofolni, L. Meda, E. Grilli, and M. Guzzi, "Room-temperature visible luminescence from silicon nanocrystals in silicon implanted SiO_2 layers," *Appl. Phys. Lett.*, vol. 66, no. 7, pp. 851–853, Feb. 1995.

[22] T. Komoda, J. Kelly, F. Cristiano, A. Nejim, P. Hemment, K. P. Homewood, R. Gwilliam, and B. J. Sealy, "Visible photoluminescence at room temperature from microcrystalline silicon precipitates in SiO_2 formed by ion implantation," *Nucl. Instrum. Methods Phys. Res. B*, vol. 96, no. 1–2, pp. 387–391, Mar. 1995.